Chemistry Proceedings

MDPI

Proceedings

Integrating diphenyl diselenide and its $MeHg^+$ detoxificant mechanism on a conceptual DFT framework

Folorunsho B. Omage,[1] Cláudia S. Oliveira, [1] Laura Orian[2]* and Joao Batista Teixeira Rocha,[1]*

[1] Departamento de Bioquímica e Biologia Molecular, Universidade Federal de Santa Maria, Santa Maria RS Brazil; omagefolorunsho@gmail.com (F.B.O.); claudia.bioquimica@yahoo.com.br (C.S.O.)

[2] Dipartimento di Scienze Chimiche Università degli Studi di Padova Via Marzolo 1 35131 Padova, Italy;

* Correspondence: laura.orian@unipd.it (L.O.); jbtrocha@gmail.com (J.B.T.R),

† Presented at the 1st International Electronic Conference on Catalysis Sciences, 15–30 November 2020; Available online: https://eccs2020.sciforum.net/

Published: 10 November 2020

Abstract: Methylmercury ($MeHg^+$) is an important environmental contaminant and its toxicity is associated with its interaction with selenium (e.g., selenol groups of selenoproteins or HSe^-, which is the pivotal metabolite for Se incorporation into selenoproteins). We hypothesized that $(PhSe)_2$ mediated $MeHg^+$ detoxification could be indirectly altered by its open or closed conformation. The two conformations of $(PhSe)_2$ were located on the potential energy surface (PES) computed at ZORA-OPBE-D3(BJ)/ZORA-def2-TZVP. HPLC analysis indicated that $(PhSe)_2$ did not react with $MeHg^+$, but its reduced intermediate formed a stable complex with $MeHg^+$. The intrinsic reaction calculations (IRC) using nudged elastic band (NEB) method, revealed conformational changes from close to open state with an H^- (2 electrons) transfer from $NaBH_4$, forming a reactant complex-like transition state (TS). The UV-Vis spectrophotometer used in combination with the time-dependent density functional theory (TD-DFT) indicated the signal of $(PhSe)_2$ at 239 nm was possibly the open state signal with oscillator strength 0.1 and a $\pi \rightarrow \pi^*$ electron transfer. The experimental band gap energy of $(PhSe)_2$ at 5.20 eV matched the excitation energy of the open conformation. The local softness (S^-) on the selenium atoms almost doubles, as state changes from closed to open. The theoretical results have indicated that the open conformation of $(PhSe)_2$ is likely the one that reacts with $NaBH_4$ to form the PhSeH, which can react with $MeHg^+$.

Keywords: diphenyl diselenide; rHPLC; TD-DFT; DFT calculations; conceptual DFT; NEB

1. Introduction

In the aquatic food web, methylmercury ($MeHg^+$) can be biomagnified and can reach toxic levels in the edible muscle of predatory or piscivorous fish [1,2]. The frequent consumption of predatory fish can result in $MeHg^+$ intoxication [2]. The toxicity of the soft electrophilic $MeHg^+$ is mediated by inactivation of proteins containing soft nucleophilic sites (e.g., thiol- and selenol-containing proteins) [3–7]. $MeHg^+$ has an extremely high affinity for –SH and –SeH groups [5,8]. Experimental and theoretical studies have indicated that the affinity of $MeHg^+$ for –SeH is greater than for –SH groups [5]. Selenium (Se) is an essential element for vertebrates as part of the selenol group present in the selenocysteine residues found in selenoproteins. In a previous study, we demonstrated that diphenyl diselenide $(PhSe)_2$ decreased the deposition of Hg in mice treated with $MeHg^+$. A decreased mercury burden in liver, kidney, cerebrum and cerebellum of mouse was reported in mice treated with $(PhSe)_2$ [3,4,9]. We have hypothesized that $(PhSe)_2$ could be reduced to its selenol intermediate PhSeH, which formed a complex with $MeHg^+$ (i.e., PhSeHgMe) [5,9,10]. The reduction of $(PhSe)_2$ and its eventual reaction with methylmercury have several intricate and interesting parts, as reactions may eventually depend on the conformation assumed by $(PhSe)_2$ in the reacting medium [11–13].

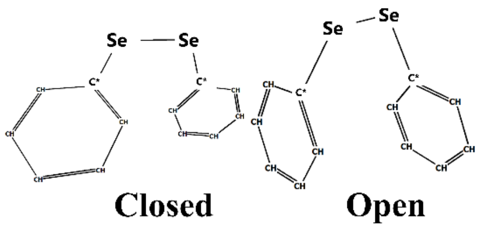

Scheme 1: Closed and open conformation of diphenyl diselenide.

$(PhSe)_2$ presents two conformations in its ground state, referred to as the closed and open conformation (Scheme 1) [12,14]. The reduction of $(PhSe)_2$ using $NaBH_4$ involves a hydride transfer via a likely single-step mechanism [15], Scheme 2. It has been reported [16] that the hydride transfer process is strongly affected by solvent, with the open state acting as the hydride acceptor from the $NaBH_4$ donor. A likely mechanism is shown in Scheme 2.

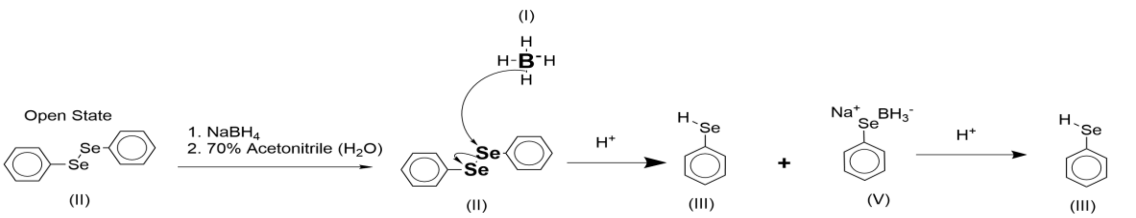

Scheme 2: Diphenyl diselenide reduction by $NaBH_4$.

The nudged elastic band (NEB) method [17] was used to locate the relevant points on the PES, i.e. the minima and transition states. TD-DFT [18] calculations were performed at ZORA-CAM-B3LYP/zora-def2-TZVP to compute the excitation energies and interpret the experimental spectrum. Then we used the conceptual density functional theory (c-DFT), [19] which involves the use of DFT, electron density to unravel the reactivity of chemical systems. Particularly, the Fukui function f(r) was computed. This function is the second derivative of energy (E) at a constant external potential, derived by perturbing the chemical system from N to N+1 and N to N-1 [20]. This function indicates the regioselectivity [21], a region on a molecule where there will be either a nucleophilic or electrophilic attack.

2. Methods

2.1. Experimental

A stock solution of 10 mM was prepared by dissolving 19.6 mg of $(PhSe)_2$ in 6.28 ml of 70% Acetonitrile, from which 5µL ($(PhSe)_2$ final concentration of 50 µM) was used in the reaction, same concentration applied to $NaBH_4$, DTT and MeHg. The UV absorption spectrum of $(PhSe)_2$ was recorded in the region of 220 nm–450 nm with 70% acetonitrile as the solvent using a UV-1800 Shimadzu spectrophotometer. Analysis of methylmercury reaction with $(PhSe)_2$ was performed using a Shimadzu SPD-20A UV/Vis Detector, CBM-20A communication bus module and DGU-20A5 Degasser prominence high-performance liquid chromatography (HPLC) controlled by the LCSolution software system. Detection was monitored at 239 nm UV wavelength. The separation was achieved on a VerticalTM VertiSep GES C18 HPLC column (4.6 x 150 mm). The mobile phase used for the analysis of the reaction was at 70% acetonitrile-0.5% phosphoric acid aqueous solution (70:30, V/V) with a flow rate of 0.8 mL/min. An injection volume of 50µL was used. The retention time was approximately 12.5 min for (PhSe)2. The peak areas were used for quantification. The estimated void volume is 1.75ml and at 0.8ml/min flow rate gives 2.19 min.

2.2. Computational Methods

All Density Functional Theory (DFT) calculations were done with ORCA 4.1.2 [22,23]. Geometry optimizations and vibrational frequencies were performed at ZORA-OPBE-D3(BJ)/ZORA-def2-TZVP [24,25] level of theory. The Zeroth-order regular approximation (ZORA) was used in order to include scalar relativistic effects due to the presence of selenium atom [26] as previously benchmarked [11]. In addition, the effect of dispersion was included using Grimme's approximation (D3(BJ)) [27,28]. The FMO (frontier molecular orbitals) energies and related parameters were obtained at ZORA-OPBE-D3(BJ)/ZORA-def2-TZVP level. The NEB analysis was carried out at ZORA-OPBE-D3(BJ)/ZORA-def2-TZVP level. The chemical reactivity descriptors used are the local softness(s), global hardness (η) and global softness (S), defined as: $\eta = (IE-EA)/2$ and $S = 1/(IE-EA)$ where IE is the Ionization Energy which corresponds to the HOMO energy taken with a negative sign and EA is the electron affinity which corresponds to the LUMO energy taken with a negative sign. The local softness is (s) = S (Global Softness) x f(r) where the Fukui function f(r) [20,29,30] is the second derivative of E at a constant external potential. The dual descriptors $f(2)(r) > 0$ indicate preferable sites for nucleophilic attack and $f(2)(r) < 0$ shows sites for electrophilic attack. The experimental band gap energy was obtained by calculating the energy using Planck-Einstein relationship $E(eV)=hc/\lambda$. The pkCSM server [31] (http://biosig.unimelb.edu.au/pkcsm/prediction) was used in predicting the total clearance(CLtot) of $(PhSe)_2$, $MeHg^+$ and MeHgSePh [32].

3. Results

A reactant-like transition state (TS) geometry according to Hammond's theory is formed, with the TS energy closer to the reaction state. The closed conformer turns into the open one before the TS.

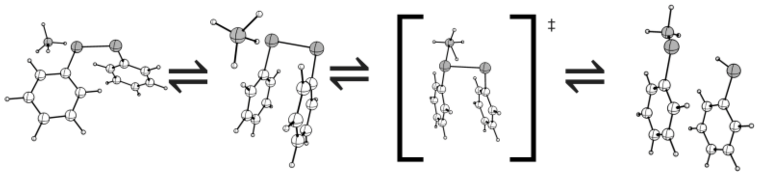

.

Scheme 3. Mechanism of $(PhSe)_2$ reduction.

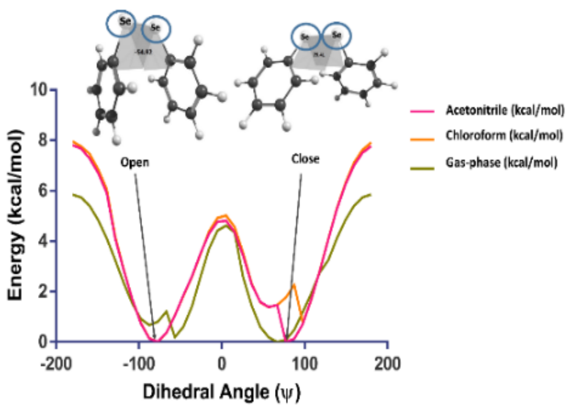

Figure 1. Potential Energy Surface (PES) scan of $(PhSe)_2$ in gas-phase and in different solvents; level of theory: ZORA-OPBE-D3(BJ)/ZORA-def2-TZVP.

The TS corresponding to the vibration of the boron-hydrogen/ hydrogen-selenium cleavage/bond formation and occurring during the transfer of the hydride ion (H-) obtained from the NEB calculation was verified with frequencies calculation at the same level of theory. (Scheme 3)

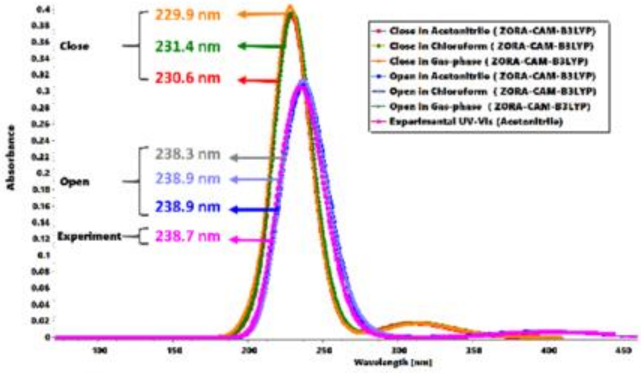

Figure 2. Computed spectra of the open and closed conformers of $(PhSe)_2$ in different media and experimental spectrum recorded in acetonitrile (pink); level of theory: ZORA-CAM-B3LYP/TZVP.

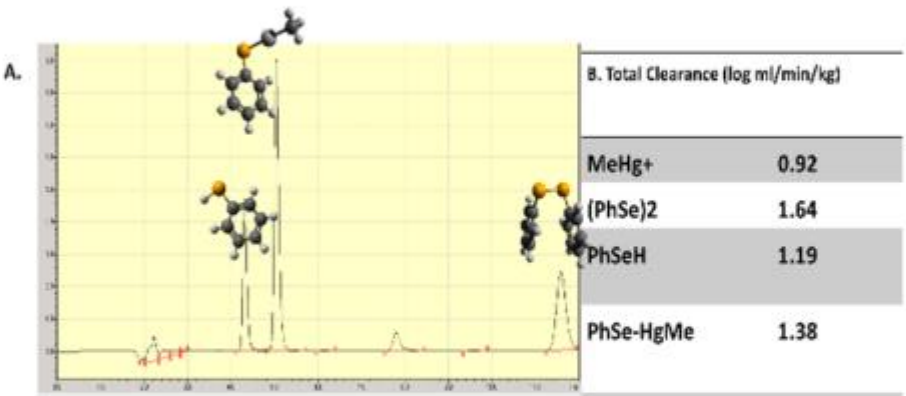

Figure 3(A). The chromatogram of $(PhSe)_2$ using VerticalTM VertiSep GES C18 HPLC column (4.6 x 150 mm) with 70% acetonitrile-0.5% phosphoric acid aqueous solution (70:30, V/V) mobile phase at a flow rate of 0.8 mL/min**. (B).** Total clearance of the reagents as predicted using pKCSM.

4. Discussion

The PES scan performed at ZORA-OPBE-D3(BJ)/ZORA-def2-TZVP level of theory across the dihedral angle ψ (C-Se-Se-C*, Scheme 1) reveals two minima corresponding to approximately -80 and + 80 degrees (Fig. 1). The spikes in the curve correspond to switches in the orientation of the phenyl rings converting the open/closed conformations. Solvation brings minimal changes, and the two minima are just slightly shifted, while the phenyl rings orientation in correspondence of these minima is maintained as in the gas-phase. The actual detoxifying of $MeHg^+$ is the selenol metabolite obtained from the reduction of $(PhSe)_2$ by two electrons transfer process (Scheme 2, Figure 4), breaking the Se-Se bond. The orientation of the phenyl rings is expected to modulate the equilibrium shift, either in favor or against the formation of selenol, hence modifying indirectly the detoxification process. Hydride transfer process are strongly affected by solvent [16]. The crystallographic structure retrieved from the Cambridge Structural Database (CSD) [33,34] is in the closed state. At ZORA-

CAM-B3LYP/zora-def2-TZVP (Figure 3) the modelled spectrum of the open state, matches to the experimental spectrum at λmax 238.7 nm, with slight difference of only 0.2 nm. The excitation energy of the open state at the same level of theory matched the experimental band gap energy of 5.2 eV. The cDFT result revealed change in susceptibility of diphenyl diselenide in the close state for nucleophilic attacks with the dual descriptor f(2)(r) > 0 (0.032) to electrophilic attacks with f(2)(r) = -0.046, with extended bond length of 5%. Change to open state increases the reactivity, with the local softness (S-) on the selenium atoms almost doubled.

5. Conclusions

In this work, we have used both experimental and theoretical approach to identify the reactive state of $(PhSe)_2$. We interpreted experimental absorption of $(PhSe)_2$ at 239 nm possibly to be the open state wavelength with a $\pi \rightarrow \pi^*$ electron transfer. The reaction with $MeHg^+$ was observed to be preceded by a reduction reaction. A hydride transfer from $NaBH_4$ to $(PhSe)_2$ open state was postulated and confirmed by locating a TS via NEB method: a reactant-like transition state (TS) geometry is formed with selenol as the product. This study provides new insight into the study of $(PhSe)_2$ use as a methylmercury detoxificant agent.

Author Contributions: Conceptualization, supervision, validation and project administration, J.B.T.R and L.O.; methodology, J.B.T.R, L.O, F.B.O, C.S.O; formal analysis, investigation and data curation, F.B.O; writing—original draft preparation, F.B.O, J.B.T.R, L.O, writing—review and editing, F.B.O, C.S.O., J.B.T.R, L.O.

Funding: JBT. R., FB.O., CS.O. and L.O. would like to thank the financial support by Coordination for IMProvement of Higher Education Personnel CAPES/PROEX (n° 23038.005848/2018-31; nº 88887.354370/2019-00), and P-DiSC 2018 MAD3S (Modeling Antioxidant Drugs: Design and Development of computer-aided molecular Systems), the CAPES/PrInt – Institutional Internationalization Project (nº 88887.374997/2019-00), ISCRA Grant MEMES (MEthylMErcury and Selenoproteins), the National Council for Scientific and Technological Development (CNPq), and the Rio Grande do Sul Foundation for Research Support (FAPERGS).

Conflicts of Interest: “The authors declare no conflict of interest.”

References

1. Farina, M.; Aschner, M. Glutathione antioxidant system and methylmercury-induced neurotoxicity: An intriguing interplay. *Biochim. Biophys. Acta-Gen. Subj.* **2019**, *1863*, 129285. doi:10.1016/j.bbagen.2019.01.007.
2. Farina, M.; Rocha, J.B.T.; Aschner, M. Mechanisms of methylmercury-induced neurotoxicity: Evidence from experimental studies. In Proceedings of the Life Sciences; 2011.
3. Glaser, V.; Moritz, B.; Schmitz, A.; Dafré, A.L.; Nazari, E.M.; Rauh Müller, Y.M.; Feksa, L.; Straliottoa, M.R.; De Bem, A.F.; Farina, M. Protective effects of diphenyl diselenide in a mouse model of brain toxicity. *Chem. Biol. Interact.* **2013**, doi:10.1016/j.cbi.2013.08.002.
4. Glaser, V.; Martins, R.D.P.; Vieira, A.J.H.; Oliveira, E.D.M.; Straliotto, M.R.; Mukdsi, J.H.; Torres, A.I.; De Bem, A.F.; Farina, M.; Da Rocha, J.B.T.; et al. Diphenyl diselenide administration enhances cortical mitochondrial number and activity by increasing hemeoxygenase type 1 content in a methylmercury-induced neurotoxicity mouse model. *Mol. Cell. Biochem.* **2014**, doi:10.1007/s11010-013-1870-9.
5. Madabeni, A.; Dalla Tiezza, M.; Omage, F.B.; Nogara, P.A.; Bortoli, M.; Rocha, J.B.T.; Orian, L. Chalcogen–mercury bond formation and disruption in model Rabenstein’s reactions: A computational analysis. *J. Comput. Chem.* **2020**, *41*, 2045–2054, doi:10.1002/jcc.26371.
6. Branco, V.; Carvalho, C. The thioredoxin system as a target for mercury compounds. *Biochim. Biophys. Acta-Gen. Subj*. **2019**.
7. Meinerz, D.F.; Branco, V.; Aschner, M.; Carvalho, C.; Rocha, J.B.T. Diphenyl diselenide protects against

methylmercury-induced inhibition of thioredoxin reductase and glutathione peroxidase in human neuroblastoma cells: a comparison with ebselen. *J. Appl. Toxicol.* **2017**, *37*, 1073–1081, doi:10.1002/jat.3458.
8. Nogara, P.A.; Oliveira, C.S.; Schmitz, G.L.; Piquini, P.C.; Farina, M.; Aschner, M.; Rocha, J.B.T. Methylmercury's chemistry: From the environment to the mammalian brain. *Biochim. Biophys. Acta-Gen. Subj.* **2019**, *1863*, 129284, doi:10.1016/j.bbagen.2019.01.006.
9. de Freitas, A.S.; Funck, V.R.; Rotta, M. dos S.; Bohrer, D.; Mörschbächer, V.; Puntel, R.L.; Nogueira, C.W.; Farina, M.; Aschner, M.; Rocha, J.B.T. Diphenyl diselenide, a simple organoselenium compound, decreases methylmercury-induced cerebral, hepatic and renal oxidative stress and mercury deposition in adult mice. *Brain Res. Bull.* **2009**, doi:10.1016/j.brainresbull.2008.11.001.
10. Oliveira, C.S.; Nogara, P.A.; Ardisson-Araújo, D.M.P.; Aschner, M.; Rocha, J.B.T.; Dórea, J.G. Neurodevelopmental Effects of Mercury. *Advances in Neurotoxicology*, **2018**, *2*, 27–86.
11. Zaccaria, F.; Wolters, L.P.; Fonseca Guerra, C.; Orian, L. Insights on selenium and tellurium diaryldichalcogenides: A benchmark DFT study. *J. Comput. Chem.* **2016**, *37*, 1672–1680, doi:10.1002/jcc.24383.
12. Bortoli, M.; Tiezza, M.D.; Muraro, C.; Saielli, G.; Orian, L. The 125Te chemical shift of diphenyl ditelluride: Chasing conformers over a flat energy surface. *Molecules* **2019**, doi:10.3390/molecules24071250.
13. Piccoli, B.C.; Alvim, J.C.; da Silva, F.D.; Nogara, P.A.; Olagoke, O.C.; Aschner, M.; Oliveira, C.S.; Rocha, J.B.T. High level of methylmercury exposure causes persisted toxicity in Nauphoeta cinerea. *Environ. Sci. Pollut. Res.* **2020**, doi:10.1007/s11356-019-06989-9.
14. Bortoli, M.; Zaccaria, F.; Tiezza, M.D.; Bruschi, M.; Guerra, C.F.; Matthias Bickelhaupt, F.; Orian, L. Oxidation of organic diselenides and ditellurides by H_2O_2 for bioinspired catalyst design. *Phys. Chem. Chem. Phys.* **2018**, *20*, 20874–20885, doi:10.1039/c8cp02748j.
15. Hydride vs. Electron Transfer in the Reduction of Flavinand Flavin Radical by 1,4-Dihydropyridines; *J.Am.Chem.Soc*. **1983**, *105*, 1014–1021.
16. Hori, Y.; Ida, T.; Mizuno, M. A comparative theoretical study of the hydride transfer mechanisms during LiAlH4 and LiBH4 reductions. *Comput. Theor. Chem.* **2016**, doi:10.1016/j.comptc.2015.12.014.
17. Jónsson, H.; Mills, G. and Jacobsen, K.W. Nudged elastic band method for finding minimum energy paths of transitions; 1998.
18. Runge, E.; Gross, E.K.U. Density-functional theory for time-dependent systems. *Phys. Rev. Lett.* **1984**, doi:10.1103/PhysRevLett.52.997.
19. Parr, R.G.; Yang, W. Density Functional Approach to the Frontier-Electron Theory of Chemical Reactivity. *J. Am. Chem. Soc.* **1984**, doi:10.1021/ja00326a036.
20. Méndez, F.; Gázquez, J.L. Chemical Reactivity of Enolate Ions: The Local Hard and Soft Acids and Bases Principle Viewpoint. *J. Am. Chem. Soc.* **1994**, doi:10.1021/ja00099a055.
21. Berger, G. Using conceptual density functional theory to rationalize regioselectivity: A case study on the nucleophilic ring-opening of activated aziridines. *Comput. Theor. Chem.* **2013**, doi:10.1016/j.comptc.2012.12.029.
22. Neese, F. The ORCA program system. *Wiley Interdiscip. Rev. Comput. Mol. Sci.* 2012, doi:10.1002/wcms.81.
23. Neese, F. The ORCA Program System: Software Opdate - Version 4.0. *Wiley Interdiscip. Rev. Comput. Mol. Sci.* **2018**, doi:10.1002/wcms.1327.
24. Swart, M.; Ehlers, A.W.; Lammertsma, K. Performance of the OPBE exchange-correlation functional. *Mol. Phys.* **2004**, doi:10.1080/0026897042000275017.

25. Weigend, F.; Ahlrichs, R. Balanced Basis Sets of Split Valence, Triple Zeta Valence and Quadruple Zeta Valence. *Phys. Chem. Chem. Phys.* **2005,** doi:10.1039/b508541a.
26. Van Lenthe, E.; Baerends, E.J.; Snijders, J.G. Relativistic total energy using regular approximations. *J. Chem. Phys.* **1994**, *101*, 9783–9792, doi:10.1063/1.467943.
27. Grimme, S.; Ehrlich, S.; Goerigk, L. Effect of the Damping Function in Dispersion Corrected Density Functional Theory. *J. Comput. Chem.* **2011**, *32*, 1456–1465, doi:10.1002/jcc.
28. Nguyen, M.T.; Creve, S.; Eriksson, L.A.; Vanquickenborne, L.G. Calculation of the hyper® ne constants of phosphorus-containing radicals. **1997**, *91*, 537–550.
29. Roos, G.; Geerlings, P.; Messens, J. Enzymatic catalysis: The emerging role of conceptual density functional theory. *J. Phys. Chem. B* **2009**, doi:10.1021/jp9034584.
30. Fukui, K. The Path of Chemical Reactions - The IRC Approach. *Acc. Chem. Res.* 1981, doi:10.1021/ar00072a001.
31. Pires, D.E.V.; Blundell, T.L.; Ascher, D.B. pkCSM: Predicting small-molecule pharmacokinetic and toxicity properties using graph-based signatures. *J. Med. Chem.* 2015, doi:10.1021/acs.jmedchem.5b00104.
32. Wilkinson, G.R. Clearance approaches in pharmacology. *Pharmacol. Rev.* **1987**, *39*, 1–47.
33. Allen, F. H. The Cambridge Structural Database: a quarter of a million crystal structures and rising. *Acta Crystallogr. Sect. B Struct. Sci.* 2002, 380–388.
34. Groom, C.R.; Bruno, I.J.; Lightfoot, M.P.; Ward, S.C. The Cambridge structural database. Acta Crystallogr. Sect. B Struct. *Sci. Cryst. Eng. Mater.* **2016**, *72*, 171–179, doi:10.1107/S2052520616003954.